Heliyon 9 (2023) e21722

Contents lists available at ScienceDirect

Heliyon

journal homepage: www.cell.com/heliyon

Dopamine as a polymerizable reagent for enzyme-linked immunosorbent assay using horseradish peroxidase

Sumed Yadoung [a], Shinichi Shimizu [b], Surat Hongsibsong [a,c,d,*], Koji Nakano [b], Ryoichi Ishimatsu [e,**]

[a] Environmental Science Program, Faculty of Science, Chiang Mai University, 50200, Thailand
[b] Department of Applied Chemistry, Graduate School of Engineering, Kyushu University, 744 Motooka, Nishi-ku, Fukuoka, 819-0395, Japan
[c] School of Health Sciences Research, Research Institute for Health Science, Chiang Mai University, Chiang Mai, 50200, Thailand
[d] Environmental, Occupational Health Sciences and Non-Communicable Diseases Center of Excellence, Research Institute for Health Sciences, Chiang Mai University, Chiang Mai, 50200, Thailand
[e] Department of Applied Physics, University of Fukui, 3-9-1 Bunkyo, Fukui, 910-8507, Japan

ARTICLE INFO

Keywords:
Catechol
Catechol amine
Enzymatic reaction
Polymerization

ABSTRACT

We demonstrate that dopamine can be used as a reagent for colorimetric enzyme-linked immunosorbent assay (ELISA) using horseradish peroxidase (HRP). Dopamine was able to be polymerized in the presence of HRP and H_2O_2, and black polydopamine was obtained after the enzymatic reaction. Because of the black color, the absorbance was significantly changed in the whole range of the visible light region. Here, an indirect competitive ELISA based on the polymerization of dopamine was performed to detect a fluoroquinolone antibiotic, enrofloxacin. The antibiotic is commonly used in livestock farming. The anti-antibiotics antibody was produced from egg yolk from chicken hens. In the visible range, sufficient absorbance changes of ~0.4~0.5 and a low background level for the ELISA response were obtained, and the 50 % inhibitory concentration value at 450 nm was determined to be 26 ppb. The performance of the indirect competitive ELISA based on the polymerization of dopamine was compared to that based on the oxidation of catechol because dopamine has a catechol skeleton. By the complex of HRP and H_2O_2, catechol can be oxidized to *o*-benzoquinone having a maximum absorption wavelength of 420 nm. It was shown that the absorbance change in the case of polydopamine was about 2.5 times higher than that of catechol, where the background levels were similar. This confirms that the polymerization of dopamine significantly enhanced the photosignal.

1. Introduction

Enzyme-linked immunosorbent assays (ELISAs), which involve antigen-antibody interaction and enzymatic reaction [1], enable highly sensitive and selective detection for analytes. The enzymes chemically attached to antigens or antibodies induce an enzymatic reaction of a substrate, and the products of the reaction, which can normally be detected by the photometric or electrochemical response, are generated. Horseradish peroxidase (HRP) is one of the popular enzymes for ELISAs. HRP can be activated by the

* Corresponding author. Environmental Science Program, Faculty of Science, Chiang Mai University, 50200, Thailand.
** Corresponding author. Department of Applied Physics, University of Fukui, 3-9-1 Bunkyo, Fukui, 910-8507, Japan.
E-mail addresses: surat.hongsibsong@cmu.ac.th (S. Hongsibsong), ishima2@u-fukui.ac.jp (R. Ishimatsu).

https://doi.org/10.1016/j.heliyon.2023.e21722
Received 19 August 2023; Received in revised form 25 October 2023; Accepted 26 October 2023
Available online 28 October 2023

substrate, H_2O_2, and the complex of HRP and H_2O_2 has a relatively high oxidation potential (~1 V) [2,3], which is attributable to the formation of Fe(VI)═O and cation of its amino acid residues. Therefore, chemicals having an oxidation potential lower than ~1 V can be oxidized in the presence of HRP and H_2O_2, and could be employed for ELISA. Color-developing reagents such as *o*-phenylenediamine (OPD) and 3,3′,5,5′-tetramethylbenzidine (TMB), and Amplex Red, which is a parent molecule of fluorescent resorufin, are frequently used for ELISAs with HRP. It has recently been reported nanozyme immunoassays [4–22], where metal nanoparticles, metal-organic frameworks, and their nanocomposites attached to antibodies or antigens work like HRP, i.e., the nanozymes can oxidize some chemicals, such as TMB, OPD, and H_2O_2. Understanding the nanozymatic reactions based on the oxidation potential of the reactants could be important in designing the detection systems. By focusing on the oxidation potential of the HRP-H_2O_2 complex, we recently developed a new ELISA system based on the polymerization reaction of aniline [23]. The oxidation potential of aniline is ~0.2 V [24], and in the ELISA system, aniline was able to be polymerized by the presence of HRP and H_2O_2. As a result, aniline oligomers showing broad absorption spectra in the visible range were produced.

A great effort has been recently dedicated to portable detection systems to enable on-site analysis and diagnosis. Combining such a portable detection system with ELISA methods realizes highly sensitive and selective on-site detections [23,25–40]. So far, we developed several portable ELISA systems based on flow injection analysis, in which a lightweight light source such as LEDs [23,36,37] and organic light-emitting diodes(OLEDs) [38] with a suitable emission wavelength to detect the enzymatic product was incorporated. Being employed as a light source, OLEDs having narrow emission spectra derived from the f-f transition by Tb [38] and Eu complexes [41] were suitable. Alternatively, a band-pass filter should be employed for photometric detection. It is necessary to focus on the stability of the color-developing reagents; for on-site analysis, stable reagents are desired. Widely used color-developing reagents such as OPD and TMB, and Amplex Red, which must be stored in a refrigerator or freezer, react automatically under ambient conditions. Therefore, more convenient chemicals should be explored.

Products of enzymatic reactions having broad absorption spectra are advantageous for colorimetric detection systems because when ELISA samples contain colored contaminants, it is possible to select various wavelengths that are out of range of the light absorption by them. Although aniline is stable under ambient conditions and the oligomer showed broad absorption spectra, in the previous research, the competitive flow ELISA with aniline resulted in a slight change in absorbance (<0.05 absorbance change) due to the formation of small amounts of the oligomers. Large absorbance changes are more favorable for colorimetric ELISAs.

Here we report the polymerization ELISA using dopamine. Dopamine can be polymerized in the presence of HRP and H_2O_2 [42]. The absorbance change caused by the formation of black polydopamine was utilized to determine the antigen. So far, polydopamine has been used as a scaffold of polystyrene nanoparticles [43], nanocomposites of Au nanoparticles and carbon nanotube [44] or graphene [45], and PbS quantum dots [46] and as a nanocomposite with metal-organic frameworks [47], Prussian blue [48], and magnetic nanoparticles [49] for immunoassays. However, as far as we know, the colorimetric response of polydopamine generated by HRP has not been incorporated into ELISA so far.

Regarding the antigen-antibody interaction, we employed some fluoroquinolones (ciprofloxacin [50] and enrofloxacin [51], the molecular structures are shown in Fig. 1) as antigens and anti-antibiotics immunoglobulin Y (IgY), which was produced from egg yolk from chicken hens. The antigen-antibody interaction between some fluoroquinolones and anti-antibiotics IgY was recently reported by our group [52]. The anti-fluoroquinolone antibody can recognize ciprofloxacin, enrofloxacin, and norfloxacin [53] selectively and sensitively. The antibody was developed to determine the antibiotics in meat products, and it was shown that ELISA with the anti-antibiotics IgY was successfully applied for meat products. In Thailand, antibiotics are commonly used in livestock farming. Also in Japan, fluoroquinolones are used in livestock farming, and in 2021, the amount of pure active substance of enrofloxacin and norfloxacin was 3457 and 2268 kg, respectively, where enrofloxacin and norfloxacin are mainly used for broilers, beef cattle, dairy cows, and pigs, and broilers and pigs, respectively [54]. Ciprofloxacin, which is an antibiotic being prescribed to humans for the treatment of bacterial infections, is a metabolite of enrofloxacin and is not used in livestock farming. The use of antibiotics in large quantities for the treatment of bacterial diseases may be resulted in contamination of the meat products, and may cause a serious food safety problem. Therefore, monitoring the level of antibiotics in meat products contributes to food safety. Although it is possible to detect fluoroquinolones in samples by chromatographic techniques [55–57], the analytical methods normally require an expensive apparatus, and cannot treat many samples simultaneously. By employing ELISA methods, one can screen many samples at the same time with relatively low costs.

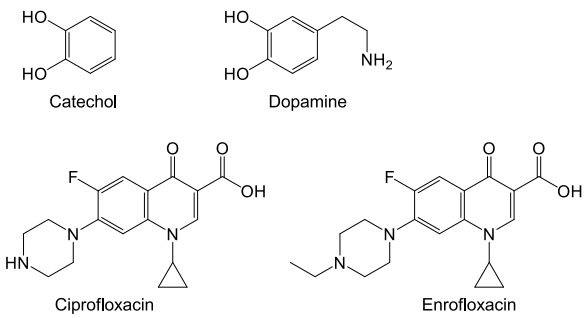

Fig. 1. Molecular structures of catechol, dopamine, and antibiotics used in this study.

2. Experimental

2.1. Chemicals and apparatus

Dopamine hydrochloric acid and catechol were purchased from Tokyo Chemical Industry Co., LTD (Tokyo, Japan). HRP, OPD, and Tween20 were received from Wako Pure Chemical Industries, Ltd. (Osaka, Japan). Ciprofloxacin and norfloxacin were obtained from Sigma-Aldrich Co. LLC (St. Louis, MO, U.S.A.). Enrofloxacin was supplied from General Drugs House Co., Ltd. (Lam Luk KA, Thailand). The horseradish peroxidase-labeled goat anti-chicken immunoglobulin (HRP-labeled anti-IgY antibody) was purchased from Invitrogen (Rockford, IL, U.S.A.).

Vis. absorption spectra were recorded on a spectrometer (V-560, JASCO Co., Tokyo, Japan). Cyclic voltammograms were acquired with an electrochemical analyzer (715AN, BSA Inc., Tokyo, Japan). Absorbance change for ELISA was monitored with a microplate reader (Infinite 200 PRO, Tecan, Austria).

2.2. Electrochemical measurements

A there-electrode system employing a glassy carbon (GC) disk (diameter: 3 mm), Pt wire, and Ag|AgCl wire as a working, counter, and reference electrode, respectively, were used to control the applied potential. Before the electrochemical measurements, the GC electrode was polished with alumina suspension (diameter: 50 nm). Cyclic voltammograms of catechol and dopamine were acquired in a phosphate buffer solution (pH = 7.0).

2.3. Visible absorption spectra of polydopamine

A mixture of HRP and dopamine or catechol dissolved in a phosphate buffer solution (pH = 7.0, 3 mL) was transferred into an optical cell, and then, a H_2O_2 solution was added into the cell. The final concentration of dopamine and catechol, and H_2O_2 were 10 and 1 mM, respectively. The final concentration of HRP to record the Vis. absorption spectra was set to 1 ppm, and that to monitor the time-dependent absorbance was changed from 0 to 100 ppb.

2.4. Indirect competitive ELISA

The details for the production of the anti-antibiotics antibody are detailed elsewhere [52]. In brief, a conjugate of bovine serum albumin and ciprofloxacin (BSA-Cip) or norfloxacin (BSA-Nor) as a hapten, which were prepared by the amine coupling method, was injected into chicken hens for several days. After immunization, the chicken eggs were collected, and the yolk was separated and purified with PEG 8000 to yield a chicken IgY anti-antibiotics antibody.

Indirect competitive ELISA based on the polymerization of dopamine was performed to detect enrofloxacin. The schematic representation of the method is shown in Fig. 2. The primary antibody (anti-antibiotics antibody) was mixed with different concentrations of antibiotics in a vial, and the solution was shaken for 60 min. A solution of coating antigen (100 μL/well, pH = 9.6) was transferred to wells of a 96-well plate and kept at 4 °C overnight. Then, the plate was washed with phosphate buffer solution with 0.05 % Tween20 (pH = 7.2) several times. To block the surface, 1 % gelatin dissolved in a phosphate buffer solution (200 μL/well) was added and incubated for 60 min. After washing, the mixture of the primary antibody and antigen (100 μL/well) was poured into the well and kept for 60 min to complete the antigen-antibody recognition. After washing with phosphate buffer (pH = 7.2), the secondary antibody (HRP-labeled anti-IgY antibody) was introduced to the wells and kept for 60 min. Then, the wells were washed gently, and finally, a mixture of H_2O_2 and dopamine or catechol was added to the wells. The color-developing time was set to 60 min.

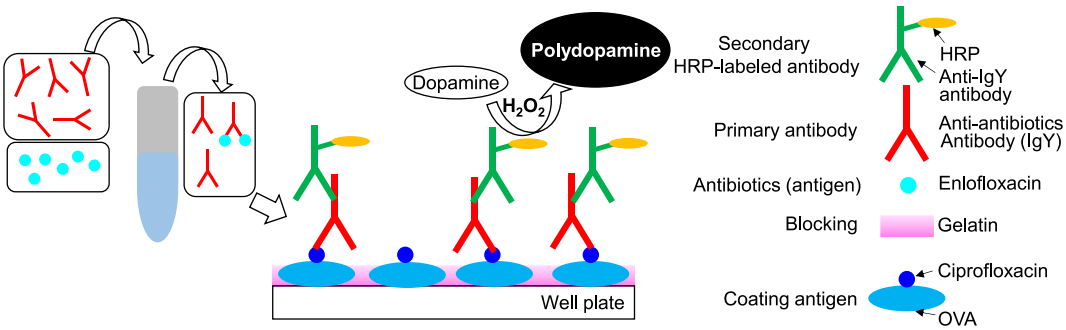

Fig. 2. Illustration of indirect competitive ELISA based on the polymerization of dopamine.

3. Results and discussion

3.1. Electrochemical properties

Fig. S1 shows cyclic voltammograms of catechol and dopamine. In the forward scan, the peak potential for catechol and dopamine appeared at 0.62 and 0.54 V vs Ag|AgCl satd. KCl, respectively. The peak potentials were much lower than the oxidation potential of the HRP-H_2O_2 complex (~1 V) [2,3]. Thus, the two compounds can energetically be oxidized in the presence of HRP and H_2O_2. By oxidation, their benzoquinone forms are produced [58]. For the two chemicals, the peak current in the backward scan was smaller than that in the forward scan. This means that the benzoquinone forms are unstable. The oxidative polymerization of dopamine is well known (see Ref. [59] and citations therein), and the polydopamine reaction is initiated by the formation of the indole form after the oxidation [60] (the most likely polymerization mechanism is shown in Scheme S1). Thus, for dopamine, the peak current in the backward scan was small because of the consumption of the benzoquinone form by the polymerization reaction. In the case of catechol, the irreversibility was caused by a nucleophilic reaction to *o*-benzoquinone. We explored the enzymatic generation of *o*-benzoquinone and polydopamine by HRP and H_2O_2 (refer to section 3.2).

3.2. Enzymatic reaction of dopamine and catechol by HRP

Fig. 3 (a) presents Vis. absorption spectra for catechol in the presence of HRP and H_2O_2 depending on the reaction time (t). The absorption spectrum for the solution containing catechol and HRP was given as $t = 0$ min. The maximum wavelength at 420 nm increased rapidly in the first 3 min after H_2O_2 was added to the solution, which indicates the generation of *o*-benzoquinone. Then, the absorbance decreased over time. The decrease coincides with the fact that *o*-benzoquinone is unstable, as was seen in the cyclic voltammogram. The time-dependent absorbance at 420 nm at different concentrations of HRP is displayed in Fig. 3 (b). For ELISAs, because the concentration of HRP reflects that of the analyte, it is important to monitor the enzymatic reaction by changing the concentration of HRP. Because the refractive index was slightly changed by mixing solutions, the absorbance decreased by adding a H_2O_2 solution. This effect was pronounced for the curve at 0 ppb HRP. As the concentration of HRP was increased, the absorbance increased. When the concentration of HRP was between 10 and 50 ppb, the absorbance increased monotonically for 600 s, whereas in the case of 100 ppb HRP, the absorbance showed a maximum of around 250 s, and then it decreased gradually. This behavior is related to the stability of *o*-benzoquinone.

For dopamine, the time-dependent Vis. absorption spectra and absorbance changes at 480 nm are shown in Fig. 4 (a) and (b), respectively. As in the case of catechol, the absorbance at 480 nm, which is attributable to the formation of the benzoquinone form, increased dramatically after the addition of H_2O_2, and then, decreased over time (Fig. 4 (a)). Moreover, at a wavelength longer than 535 nm, the absorbance was incremented with the reaction time. During the reaction, the color of the solution turned black. This

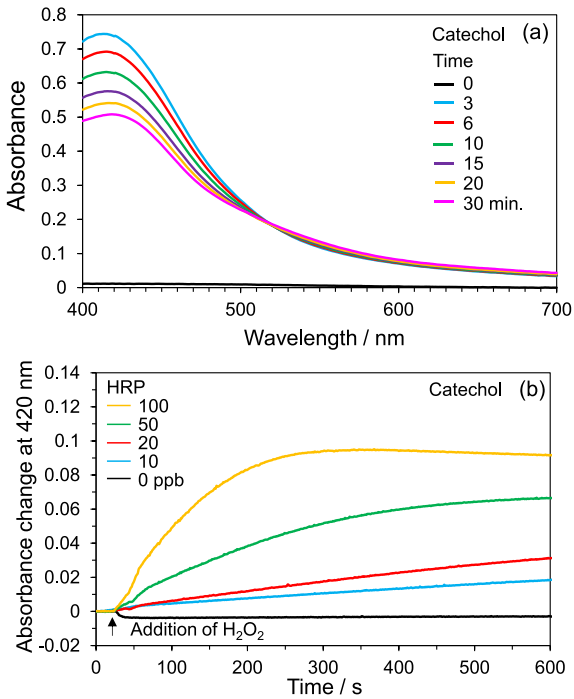

Fig. 3. (a) Vis. absorption spectra for the enzymatic reaction of 10 mM catechol by 1 ppm HRP with 1 mM H_2O_2 at different reaction times, and (b) absorbance change at 420 nm for the enzymatic reaction of catechol at different concentrations of HRP recorded in phosphate buffer (pH = 7.0).

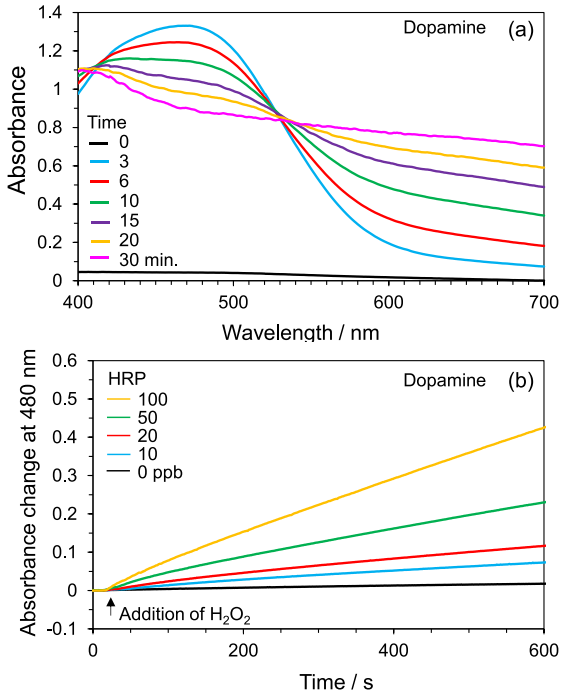

Fig. 4. (a) Vis. absorption spectra for the enzymatic reaction of 10 mM dopamine by 1 ppm HRP with 1 mM H_2O_2 at different reaction times, and (b) absorbance change at 480 nm for the enzymatic reaction of dopamine at different concentrations of HRP recorded in phosphate buffer (pH = 7.0).

confirms that the polymerization reaction proceeded to yield polydopamine (Fig. S2 shows photographs and microscopic images of the solution during the enzymatic reaction). The solution became slightly suspended as the polymerization proceeded. Thus the obtained absorbance change involves light scattering by the polydopamine aggregates somewhat. The absorbance at 420 and 480 nm between 3 and 30 min was nearly constant, which can be regarded as isosbestic points. The slight deviation may be brought by the light scattering by the aggregates. The absorbance change at 480 nm against time (Fig. 4 (b)) monotonically increased at the concentration of HRP between 10–100 ppb. Even at such low HRP concentrations, the solution color turned black, which indicates that polydopamine was formed.

Fig. 5 presents the initial velocity of the absorbance change against the concentration of HRP. The values were calculated from the absorbance change for 15 s after adding H_2O_2 in Figs. 3 (b) and 4 (b). The initial velocity was increased linearly against the concentration of HRP, and it was shown that dopamine showed a larger initial velocity of the absorbance compared to the case for catechol; the slope for dopamine in Fig. 5 is almost twice that for catechol. Because the oxidation potential of catechol and dopamine is similar, it is expected that the rate constant could be in the same degree for the oxidation of the two compounds by the HRP-H_2O_2 complex. Hence, it is highly likely that the larger absorbance change (initial velocity) in the case of dopamine is related to the formation of polydopamine. It is possible to estimate a rate constant of the enzymatic generation of *o*-benzoquinone. With the molar extinction coefficient of *o*-benzoquinone (~1400 M^{-1} cm^{-1} [61]), the slope in the case of catechol in Fig. 5 corresponds to 3.6 nM

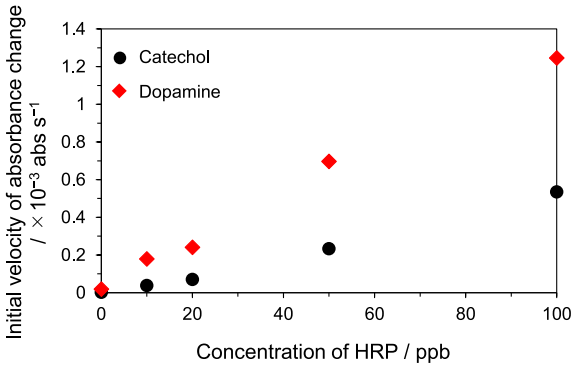

Fig. 5. Initial velocity (absorbance change) against the concentration of HRP.

ppb^{-1} s^{-1}. When the concentration of HRP is much lower than that of H_2O_2, it is reasonably assumed a steady state of the HRP-H_2O_2 complex. Then the generation of *o*-benzoquinone may be written as.

$$\text{HRP–H}_2\text{O}_2 + \text{Catechool} \rightarrow o\text{–Benzoquinone} \tag{1}$$

The rate of the formation of *o*-benzoquinone may be written as a bimolecular reaction as,

$$\frac{d[o\text{–Benzoquinon}]}{dt} = k_{app}[\text{HRP–H}_2\text{O}_2][\text{Catechol}] \tag{2}$$

were k_{app} is an apparent rate constant of the enzymatic oxidation of catechol (generation of *o*-benzoquinone) by the HRP-H_2O_2 complex. By using the molecular weight of HRP (40 kDa) and by assuming the concentration of the HRP-H_2O_2 complex as that of HRP, k_{app} for the oxidation of catechol was determined to be 1.5×10^4 M^{-1} s^{-1}. There are several reports about the k_{app} values; the substrate-dependent values were in the range of 10^2–10^7 M^{-1} s^{-1} [62–64].

Although the color change for catechol and dopamine caused by the HRP-H_2O_2 complex can be incorporated into colorimetric ELISAs, a larger absorbance change is favorable. Therefore, we hereafter focus on the polymerization ELISA using dopamine. Here we performed the indirect competitive ELISA (Fig. 2).

3.3. Indirect competitive ELISA based on polymerization of dopamine

To enhance the absorbance change in ELISA, the concentration of dopamine and H_2O_2, and pH for the enzymatic reaction, and the concentration of coating antigen, primary antibody, and secondary antibody for the antigen-antibody interaction were optimized, and we finally obtained 200 mM dopamine and 25 mM H_2O_2 at pH = 7.0 for the enzymatic reaction, 100 ppm of coating antigen, 100 ppm primary antibody, and 10 ppm secondary antibody for the antigen-antibody recognitions as the optimal condition. The details for the optimization were discussed in Supplementary (Figs. S3–S8). There are several methods for ELISA, such as sandwich, competitive, direct, and indirect types. For small molecules, normally competitive indirect or direct ELISA is employed. We chose indirect competitive ELISA for the determination of enrofloxacin because the chemical modification of the anti-antibiotics antibody can be omitted. In the case of indirect ELISA, we could not detect antibiotics (antigen) because the blocking reagents such as BAS, ovalbumin (OVA), and gelatin, which can reduce the non-specific adsorption of the primary and secondary antibodies on the substrate, are tremendously large compared to the molecular size of the antibiotics, and the antigen-antibody interaction was sterically hindered.

Fig. 6 shows the results of indirect competitive ELISA based on the polymerization of dopamine. The absorbance values at 450 and 650 nm were plotted against the concentration of the antigen, enrofloxacin. By recording the absorbance at the two wavelengths in the blue and red region as a representative, we expected the ELISA response in the visible range to be revealed. Here, as a coating antigen, ciprofloxacin-modified OVA (OVA-Cip) was chosen because, in a previous report, the combination of OVA-Cip as a coating antigen and enrofloxacin as an antigen showed the best 50 % inhibitory concentration (IC50) value among several combination ways of the coating antigen and antigen [52]. A sigmoidal curve, which is a typical response for the competitive indirect ELISA, was obtained for the two wavelengths. From the fitting for the curve, the IC50 value was determined to be 26 and 20 ppb at 450 and 650 nm, respectively. Importantly, large absorbance changes (~0.4–0.5) with relatively small standard deviations were seen in the sigmoidal curves; the absorbance was 0.720 ± 0.050 and 0.173 ± 0.002 at 450 nm for 0 and 20 ppm, respectively, and 0.555 ± 0.046 and 0.107 ± 0.001 at 650 nm for 0 and 20 ppm, respectively. Although the absorbance at 650 nm was slightly lower than that at 450 nm, their IC50 values are comparable but better somewhat compared to the previous result (50 ppb) obtained by using OPD [52]. At high concentrations of the antigen, the nonspecifically adsorbed secondary HRP-labeled antibodies cause the polymerization reaction and increase the absorbance. By considering the baseline of the absorbance (~0.05, Fig. S3) and the absorbance change by auto-polymerization (~0.03, Fig. S3), the nonspecifically adsorbed HRP-labeled antibodies are responsible for the absorbance of ~0.09 in the total absorbance of ~0.17 at 450 nm when the antigen concentration is 10~20 ppm. A typical absorption spectrum recorded after the indirect competitive ELISA is shown in Fig. S9. This confirms that in the whole visible region, the absorbance increased by the enzymatic polymerization.

We performed indirect competitive ELISA using catechol as a color-developing reagent under the optimal conditions as in the case of dopamine. The IC50 value was determined to be 28 ppb, where the absorbance at 450 nm was plotted against the concentration of enrofloxacin (Fig. S10). Although the IC50 value is comparable to that for dopamine, the absorbance on the sigmoidal curve was only changed from 0.171 ± 0.002 at 20 ppm to 0.263 ± 0.003 at 0 ppb, which is significantly small compared to the absorbance change in the case of dopamine. As in the case of dopamine, the absorbance change of ~0.04 by the auto-oxidation reaction of catechol (Fig. S11) and the baseline absorbance (~0.05) was included in the total absorbance in the ELISA results. It is natural that because of no light absorption at 650 nm for enzymatically generated *o*-benzoquinone, no appreciable absorbance change was observed at the wavelength. It should be noted that the absorbance at 10–20 ppm on the sigmoidal curves in the case of using dopamine (and also catechol) was much smaller than that using OPD (Fig. S12). The Vis. absorption spectrum obtained after the indirect competitive ELISA using OPD is displayed in Fig. S13. Overall, the comparison between the results for dopamine and hydroquinone confirms that the polymerization reaction was highly effective in increasing the absorbance and widening the detection wavelength.

4. Conclusions

A polymerization ELISA method was proposed based on the enzymatic formation of polydopamine by HRP. Because of the high oxidation potential of the HRP-H_2O_2 complex, the complex can oxidize dopamine, and the oxidation of dopamine can initiate the polymerization reaction to produce polydopamine, which shows a broad Vis. absorption spectrum. Anti-antibiotics IgY antibodies

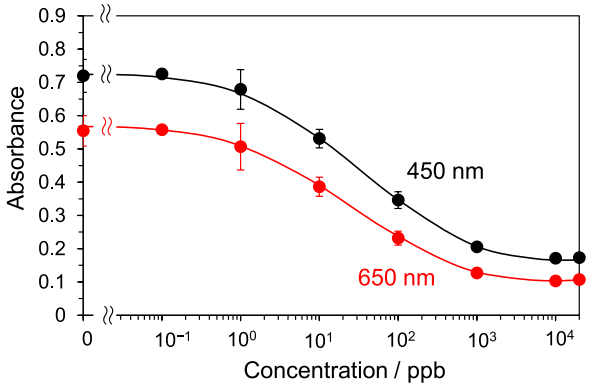

Fig. 6. Indirect competitive ELISA for the determination of enrofloxacin based on the formation of polydopamine. Absorbance caused by light absorption of polydopamine at 450 and 650 nm were plotted. The vertical bars represent the standard deviations, which were calculated from the results of triplicate measurements.

produced by a chicken hen were used to detect a fluoroquinolone antibiotic, enrofloxacin, frequently used in livestock farming. The detection wavelength of the enzymatically generated polydopamine was set to 450 and 650 nm, and sufficient absorbance changes with a reasonably low level of the baseline at the wavelengths were obtained. This indicates that the developed system covers a wide range of wavelengths, and it is possible to employ various wavelengths in the visible region. This feature is of importance when ELISA samples contain colored contaminants. The stability of dopamine, which was confirmed by a small degree of the auto-polymerization reaction, suggests that dopamine as a color-developing reagent is promising for on-site analysis.

Data availability statement

Data included in article/supp. material/referenced in article.

CRediT authorship contribution statement

Sumed Yadoung: Data curation, Formal analysis, Investigation, Visualization, Writing – original draft, Writing – review & editing. **Shinichi Shimizu:** Data curation, Formal analysis, Investigation. **Surat Hongsibsong:** Conceptualization, Data curation, Funding acquisition, Investigation, Methodology, Project administration, Supervision, Validation, Writing – original draft, Writing – review & editing. **Koji Nakano:** Resources, Writing - original draft, Writing - review & editing. **Ryoichi Ishimatsu:** Formal analysis, Investigation, Methodology, Project administration, Resources, Supervision, Validation, Visualization, Conceptualization, Writing - original draft, Writing - review & editing.

Declaration of competing interest

The authors declare that they have no known competing financial interests or personal relationships that could have appeared to influence the work reported in this paper.

Acknowledgments

This research project was supported by Fundamental Fund 2023, Chiang Mai University, Thailand. We thank Prof. Takeshi Mori (Kyushu Univ.) for his help with the measurements using the plate reader.

Appendix A. Supplementary data

Supplementary data to this article can be found online at https://doi.org/10.1016/j.heliyon.2023.e21722.

References

[1] S. Aydin, A short history, principles, and types of ELISA, and our laboratory experience with peptide/protein analyses using ELISA, Peptides 72 (2015) 4–15, https://doi.org/10.1016/j.peptides.2015.04.012.

[2] J. Hernández-Ruiz, R.N.F. Thorneley, F. García-Cánovas, A.N.P. Hiner, D.J. Lowe, J.N. Rodríguez-López, Mechanism of reaction of hydrogen peroxide with horseradish peroxidase: identification of intermediates in the catalytic cycle, J. Am. Chem. Soc. 123 (2002) 11838–11847, https://doi.org/10.1021/ja011853+.

[3] N.C. Boaz, S.R. Bell, J.T. Groves, Ferryl protonation in oxoiron(IV) porphyrins and its role in oxygen transfer, J. Am. Chem. Soc. 137 (2015) 2875–2885, https://doi.org/10.1021/ja508759t.

[4] D. Duan, K. Fan, D. Zhang, S. Tan, M. Liang, Y. Liu, J. Zhang, P. Zhang, W. Liu, X. Qiu, G.P. Kobinger, G. Fu Gao, X. Yan, Nanozyme-strip for rapid local diagnosis of Ebola, Biosens. Bioelectron. 74 (2015) 134–141, https://doi.org/10.1016/j.bios.2015.05.025.

[5] Z. Yu, Y. Tang, G. Cai, R. Ren, D. Tang, Paper electrode-based flexible pressure sensor for point-of-care immunoassay with digital multimeter, Anal. Chem. 91 (2019) 1222–1226, https://doi.org/10.1021/acs.analchem.8b04635.

[6] X. Zhang, D. Wu, Y. Wu, G. Li, Bioinspired nanozyme for portable immunoassay of allergenic proteins based on A smartphone, Biosens. Bioelectron. 172 (2021), https://doi.org/10.1016/j.bios.2020.112776.

[7] P.A. Kotelnikova, A.M. Iureva, M.P. Nikitin, A.V. Zvyagin, S.M. Deyev, V.O. Shipunova, Peroxidase-like activity of silver nanowires and its application for colorimetric detection of the antibiotic chloramphenicol, Talanta Open 6 (2022), 100164, https://doi.org/10.1016/j.talo.2022.100164.

[8] Z.J. Chen, Z. Huang, Y.M. Sun, Z.L. Xu, J. Liu, The most active oxidase-mimicking Mn_2O_3 nanozyme for biosensor signal generation, Chem. Eur J. 27 (2021) 9597–9604, https://doi.org/10.1002/chem.202100567.

[9] Z. Xu, L.-l Long, Y. qiu Chen, M.L. Chen, Y.H. Cheng, A nanozyme-linked immunosorbent assay based on metal–organic frameworks (MOFs) for sensitive detection of aflatoxin B1, Food Chem. 338 (2021), 128039, https://doi.org/10.1016/j.foodchem.2020.128039.

[10] H. Yan, Y. Chen, L. Jiao, W. Gu, C. Zhu, Amorphous $RuTe_2$ nanorods as efficient peroxidase mimics for colorimetric immunoassay, Sensor. Actuator. B Chem. 341 (2021), 130007, https://doi.org/10.1016/j.snb.2021.130007.

[11] I.M. Khoris, T. Kenta, A.B. Ganganboina, E.Y. Park, Pt-embodiment ZIF-67-derived nanocage as enhanced immunoassay for infectious virus detection, Biosens. Bioelectron. 215 (2022), 114602, https://doi.org/10.1016/j.bios.2022.114602.

[12] X. Wang, M. Zhang, X. Pang, K. Huang, Z. Yao, X. Mei, N. Cheng, Comparative study of Pd@Pt nanozyme improved colorimetric N-ELISA for the paper-output portable detection of Staphylococcus aureus, Talanta 247 (2022), 123503, https://doi.org/10.1016/j.talanta.2022.123503.

[13] D. Lee, N. Asmare, A.F. Sarioglu, Paper-based multi-well depletion ELISA, Lab Chip 23 (2022) 251–260, https://doi.org/10.1039/d2lc00960a.

[14] S. Huang, W. Lai, B. Liu, M. Xu, J. Zhuang, D. Tang, Y. Lin, Colorimetric and photothermal dual-mode immunoassay of aflatoxin B1 based on peroxidase-like activity of Pt supported on nitrogen-doped carbon, Spectrochim. Acta Part A Mol. Biomol. Spectrosc. 284 (2023), 121782, https://doi.org/10.1016/j.saa.2022.121782.

[15] Y. Su, D. Wu, J. Chen, G. Chen, N. Hu, H. Wang, P. Wang, H. Han, G. Li, Y. Wu, Ratiometric surface enhanced Raman scattering immunosorbent assay of allergenic proteins via covalent organic framework composite material based nanozyme tag triggered Raman signal "turn-on" and amplification, Anal. Chem. 91 (2019) 11687–11695, https://doi.org/10.1021/acs.analchem.9b02233.

[16] X. Ruan, D. Liu, X. Niu, Y. Wang, C.D. Simpson, N. Cheng, D. Du, Y. Lin, 2D graphene oxide/Fe-mof nanozyme nest with superior peroxidase-like activity and its application for detection of woodsmoke exposure biomarker, Anal. Chem. 91 (2019) 13847–13854, https://doi.org/10.1021/acs.analchem.9b03321.

[17] D. Xu, K. Ge, Y. Chen, S. Qi, Y. Tian, S. Wang, J. Qiu, X. Wang, Q. Dong, Q. Liu, Cobalt-Iron mixed-metal-organic framework (Co_3Fe-MMOF) as peroxidase mimic for highly sensitive enzyme-linked immunosorbent assay (ELISA) detection of Aeromonas hydrophila, Microchem. J. 154 (2020), 104591, https://doi.org/10.1016/j.microc.2019.104591.

[18] Z. Xi, W. Gao, X. Xia, Size effect in Pd−Ir core-shell nanoparticles as nanozymes, Chembiochem 21 (2020) 2440–2444, https://doi.org/10.1002/cbic.202000147.

[19] L. Wu, M. Zhang, L. Zhu, J. Li, Z. Li, W. Xie, Nanozyme-linked immunosorbent assay for porcine circovirus type 2 antibody using $HAuCl_4/H_2O_2$ coloring system, Microchem. J. 157 (2020), 105079, https://doi.org/10.1016/j.microc.2020.105079.

[20] J. Xie, M.Q. Tang, J. Chen, Y.H. Zhu, C.B. Lei, H.W. He, X.H. Xu, A sandwich ELISA-like detection of C-reactive protein in blood by citicoline-bovine serum albumin conjugate and aptamer-functionalized gold nanoparticles nanozyme, Talanta 217 (2020), 121070, https://doi.org/10.1016/j.talanta.2020.121070.

[21] S.K. Gurmessa, L.T. Tufa, J. Kim, K.I. Lee, Y.M. Kim, V.T. Tran, H.Q. Nguyen, T.S. Shim, J. Kim, T.J. Park, J. Lee, H.J. Kim, Colorimetric detection of Mycobacterium tuberculosis ESX-1 substrate protein in clinical samples using Au@Pd nanoparticle-based magnetic enzyme-linked immunosorbent assay, ACS Appl. Nano Mater. 4 (2021) 539–549, https://doi.org/10.1021/acsanm.0c02833.

[22] L. Ding, X. Shao, M. Wang, H. Zhang, L. Lu, Dual-mode immunoassay for diethylstilbestrol based on peroxidase activity and photothermal effect of black phosphorus-gold nanoparticle nanohybrids, Anal. Chim. Acta 1187 (2021), 339171, https://doi.org/10.1016/j.aca.2021.339171.

[23] R. Ishimatsu, S. Shimizu, S. Hongsibsong, K. Nakano, C. Malasuk, Y. Oki, K. Morita, Enzyme-linked immunosorbent assay based on light absorption of enzymatically generated aniline oligomer: flow injection analysis for 3-phenoxybenzoic acid with anti-3-phenoxybenzoic acid monoclonal antibody, Talanta 218 (2020), 121102, https://doi.org/10.1016/j.talanta.2020.121102.

[24] Y. Wei, Y. Sun, X. Tang, Autoacceleration and kinetics of electrochemical polymerization of aniline, J. Phys. Chem. 93 (1989) 4878–4881, https://doi.org/10.1021/j100349a039.

[25] K.E. Sapsford, J. Francis, S. Sun, Y. Kostov, A. Rasooly, Miniaturized 96-well ELISA chips for staphylococcal enterotoxin B detection using portable colorimetric detector, Anal. Bioanal. Chem. 394 (2009) 499–505, https://doi.org/10.1007/s00216-009-2730-z.

[26] A. Zhdanov, J. Keefe, L. Franco-Waite, K.R. Konnaiyan, A. Pyayt, Mobile phone based ELISA (MELISA), Biosens, Bioelectron 103 (2018) 138–142, https://doi.org/10.1016/j.bios.2017.12.033.

[27] L. Zhong, J. Sun, Y. Gan, S. Zhou, Z. Wan, Q. Zou, K. Su, P. Wang, Portable smartphone-based colorimetric analyzer with enhanced gold nanoparticles for on-site tests of seafood safety, Anal. Sci. 35 (2019) 133–140, https://doi.org/10.2116/analsci.18P184.

[28] J. Lee, H. Kim, Y. Heo, Y.K. Yoo, S. Il Han, C. Kim, D. Hur, H. Kim, J.Y. Kang, J.H. Lee, Enhanced paper-based ELISA for simultaneous EVs/exosome isolation and detection using streptavidin agarose-based immobilization, Analyst 145 (2020) 157–164, https://doi.org/10.1039/c9an01140d.

[29] R. Afriat, D. Chalupowicz, E. Eltzov, Development of a point-of-care technology for bacterial identification in milk, Talanta 219 (2020), 121223, https://doi.org/10.1016/j.talanta.2020.121223.

[30] G.W.H. Evans, W.T. Bhuiyan, S. Pang, B. Warren, K. Makris, S. Coleman, S.U. Hassan, X. Niu, A portable droplet microfluidic device for cortisol measurements using a competitive heterogeneous assay, Analyst 146 (2021) 4535–4544, https://doi.org/10.1039/d1an00671a.

[31] M. Kagawa, K. Morioka, M. Osashima, A. Hemmi, S. Yamamoto, A. Shoji, K. Uchiyama, H. Nakajima, Development of small-sized fluorescence detector for pipette tip-based biosensor for on-site diagnosis, Talanta 256 (2023), 124311, https://doi.org/10.1016/j.talanta.2023.124311.

[32] C. Liang, B. Liu, J. Li, J. Lu, E. Zhang, Q. Deng, L. Zhang, R. Chen, Y. Fu, C. Li, T. Li, A nanoenzyme linked immunochromatographic sensor for rapid and quantitative detection of SARS-CoV-2 nucleocapsid protein in human blood, Sensor. Actuator. B Chem. 349 (2021), 130718, https://doi.org/10.1016/j.snb.2021.130718.

[33] L. Yu, C.M. Li, Y. Liu, J. Gao, W. Wang, Y. Gan, Flow-through functionalized PDMS microfluidic channels with dextran derivative for ELISAs, Lab Chip 9 (2009) 1243–1247, https://doi.org/10.1039/b816018j.

[34] B.S. Lee, J.N. Lee, J.M. Park, J.G. Lee, S. Kim, Y.K. Cho, C. Ko, A fully automated immunoassay from whole blood on a disc, Lab Chip 9 (2009) 1548–1555, https://doi.org/10.1039/b820321k.

[35] J. Tian, X. Li, W. Shen, Printed two-dimensional micro-zone plates for chemical analysis and ELISA, Lab Chip 11 (2011) 2869–2875, https://doi.org/10.1039/c1lc20374f.

[36] M. Miyake, H. Nakajima, A. Hemmi, M. Yahiro, C. Adachi, N. Soh, R. Ishimatsu, K. Nakano, K. Uchiyama, T. Imato, Performance of an organic photodiode as an optical detector and its application to fluorometric flow-immunoassay for IgA, Talanta 96 (2012) 132–139, https://doi.org/10.1016/j.talanta.2012.02.006.

[37] R. Ishimatsu, A. Naruse, R. Liu, K. Nakano, M. Yahiro, C. Adachi, T. Imato, An organic thin film photodiode as a portable photodetector for the detection of alkylphenol polyethoxylates by a flow fluorescence-immunoassay on magnetic microbeads in a microchannel, Talanta 117 (2013) 139–145, https://doi.org/10.1016/j.talanta.2013.08.044.

[38] R. Liu, R. Ishimatsu, M. Yahiro, C. Adachi, K. Nakano, T. Imato, Fluorometric flow-immunoassay for alkylphenol polyethoxylates on a microchip containing a fluorescence detector comprised of an organic light emitting diode and an organic photodiode, Talanta 134 (2015) 37–47, https://doi.org/10.1016/j.talanta.2014.10.055.

[39] M. Angelopoulou, A. Botsialas, A. Salapatas, P.S. Petrou, W. Haasnoot, E. Makarona, G. Jobst, D. Goustouridis, A. Siafaka-Kapadai, I. Raptis, K. Misiakos, S. E. Kakabakos, Assessment of goat milk adulteration with a label-free monolithically integrated optoelectronic biosensor, Anal. Bioanal. Chem. 407 (2015) 3995–4004, https://doi.org/10.1007/s00216-015-8596-3.
[40] X. Ma, Y. Lin, L. Guo, B. Qiu, G. Chen, H. hao Yang, Z. Lin, A universal multicolor immunosensor for semiquantitative visual detection of biomarkers with the naked eyes, Biosens. Bioelectron. 87 (2017) 122–128, https://doi.org/10.1016/j.bios.2016.08.021.
[41] R. Liu, R. Ishimatsu, M. Yahiro, C. Adachi, K. Nakano, T. Imato, Photometric flow injection determination of phosphate on a PDMS microchip using an optical detection system assembled with an organic light emitting diode and an organic photodiode, Talanta 132 (2015) 96–105, https://doi.org/10.1016/j.talanta.2014.08.057.
[42] M. Dai, T. Huang, L. Chao, Q. Xie, Y. Tan, C. Chen, W. Meng, Horseradish peroxidase-catalyzed polymerization of l-DOPA for mono-/bi-enzyme immobilization and amperometric biosensing of H_2O_2 and uric acid, Talanta 149 (2016) 117–123, https://doi.org/10.1016/j.talanta.2015.11.047.
[43] X. Zhang, M. Liu, M. Yang, W. Cheng, J. Xiang, W. Zhu, X. Chen, Functional lightweight polystyrene@polydopamine nanoparticle for high-performance ELISA, Talanta 252 (2023), 123871, https://doi.org/10.1016/j.talanta.2022.123871.
[44] G. Wang, H. Huang, G. Zhang, X. Zhang, B. Fang, L. Wang, Dual amplification strategy for the fabrication of highly sensitive interleukin-6 amperometric immunosensor based on poly-dopamine, Langmuir 27 (2011) 1224–1231, https://doi.org/10.1021/la1033433.
[45] G. Wang, X. He, L. Chen, Y. Zhu, X. Zhang, Ultrasensitive IL-6 electrochemical immunosensor based on Au nanoparticles-graphene-silica biointerface, Colloids Surf. B Biointerfaces 116 (2014) 714–719, https://doi.org/10.1016/j.colsurfb.2013.11.015.
[46] G.A. Ortega, J.C. Zuaznabar-Gardona, E. Reguera, Electrochemical immunoassay for the detection of IgM antibodies using polydopamine particles loaded with PbS quantum dots as labels, Biosens. Bioelectron. 116 (2018) 30–36, https://doi.org/10.1016/j.bios.2018.05.046.
[47] R. Ren, G. Cai, Z. Yu, Y. Zeng, D. Tang, Metal-polydopamine framework: an innovative signal-generation tag for colorimetric immunoassay, Anal. Chem. 90 (2018) 11099–11105, https://doi.org/10.1021/acs.analchem.8b03538.
[48] X. Zhu, J. Shan, L. Dai, F. Shi, J. Wang, H. Wang, Y. Li, D. Wu, H. Ma, Q. Wei, H. Ju, PB@PDA nanocomposites as nanolabels and signal reporters for separate-type cathodic photoelectrochemical immunosensors in the detection of carcinoembryonic antigens, Talanta 254 (2023), 124134, https://doi.org/10.1016/j.talanta.2022.124134.
[49] J. Zhao, Z. Wang, Y. Chen, D. Peng, Y. Xianyu, Horseradish peroxidase-catalyzed formation of polydopamine for ultra-sensitive magnetic relaxation sensing of aflatoxin B1, J. Hazard Mater. 419 (2021), 126403, https://doi.org/10.1016/j.jhazmat.2021.126403.
[50] P.C. Sharma, A. Jain, S. Jain, R. Pahwa, M.S. Yar, Ciprofloxacin: review on developments in synthetic, analytical, and medicinal aspects, J. Enzym. Inhib. Med. Chem. 25 (2010) 577–589, https://doi.org/10.3109/14756360903373350.
[51] Ł. Grabowski, L. Gaffke, K. Pierzynowska, Z. Cyske, M. Choszcz, G. Węgrzyn, A. Węgrzyn, Enrofloxacin—the ruthless killer of eukaryotic cells or the last hope in the fight against bacterial infections? Int. J. Mol. Sci. 23 (2022) https://doi.org/10.3390/ijms23073648.
[52] S. Yadoung, R. Ishimatsu, Z.L. Xu, K. Sringarm, S. Pata, M. Thongkham, S. Chantara, M. Pattarawarapan, S. Hongsibsong, Development of IgY-based indirect competitive ELISA for the detection of fluoroquinolone residues in chicken and pork samples, Antibiotics 11 (2022), https://doi.org/10.3390/antibiotics11111512.
[53] L. Chierentin, H.R.N. Salgado, Review of properties and analytical methods for the determination of norfloxacin, Crit. Rev. Anal. Chem. 46 (2016) 22–39, https://doi.org/10.1080/10408347.2014.941456.
[54] Sales amounts and sales volumes (active substance) of antibiotics, synthetic antibacterials, anthelmintics and antiprotozoals, annual report of sales amount and sales volume of veterinary drugs, quasi-drugs, medical devices and regenerative medicine products, National Veterinary Assay Laboratory, Ministry of Agriculture, Forestry & Fisheries of Japan (2021).
[55] E. de O. Araujo, A.M. Rosa, M.S. Do Amaral, R.A. Sversut, A.C. de M. Baroni, L.C.S. de Oliveira, N.M. Kassab, Stability-indicating HPLC-DAD method for the simultaneous determination of fluoroquinolone in combination with a non-steroidal anti-inflammatory drug in pharmaceutical formulation, Brazilian J. Pharm. Sci. 56 (2020), https://doi.org/10.1590/s2175-97902019000417758.
[56] B. Shao, X. Jia, Y. Wu, J. Hu, X. Tu, J. Zhang, Multi-class confirmatory method for analyzing trace levels of tetracyline and quinolone antibiotics in pig tissues by ultra-performance liquid chromatography coupled with tandem mass spectrometry, Rapid Commun. Mass Spectrom. 21 (2007) 3487–3496, https://doi.org/10.1002/rcm.3236.
[57] K.M. Patel, B.N. Suhagia, I. Singhvi, Analytical method development and validation for enrofloxacin in bulk and formulation by RP-HPLC method, Am. J. PharmTech Res. 8 (2018) 176–185, https://doi.org/10.46624/ajptr.2018.v8.i2.013.
[58] E. Arkan, C. Karami, R. Rafipur, Immobilization of tyrosinase on Fe3o4@Au core–shell nanoparticles as bio-probe for detection of dopamine, phenol and catechol, J. Biol. Inorg. Chem. 24 (2019) 961–969, https://doi.org/10.1007/s00775-019-01691-0.
[59] W. Zheng, H. Fan, L. Wang, Z. Jin, Oxidative self-polymerization of dopamine in an acidic environment, Langmuir 31 (2015) 11671–11677, https://doi.org/10.1021/acs.langmuir.5b02757.
[60] M. D'Ischia, A. Napolitano, A. Pezzella, P. Meredith, T. Sarna, Chemical and structural diversity in eumelanins: unexplored bio-optoelectronic materials, Angew. Chemie - Int. Ed. 48 (2009) 3914–3921, https://doi.org/10.1002/anie.200803786.
[61] G. Albarran, W. Boggess, V. Rassolov, R.H. Schuler, Absorption spectrum, mass spectrometric properties, and electronic structure of 1,2-benzoquinone, J. Phys. Chem. A. 114 (2010) 7470–7478, https://doi.org/10.1021/jp101723s.
[62] M.J.H. Van Haandel, I.M.C.M. Rietjens, A.E.M.F. Soffers, C. Veeger, J. Vervoort, S. Modi, M.S. Mondal, P.K. Patel, D.V. Behere, Computer calculation-based quantitative structure-activity relationships for the oxidation of phenol derivatives horseradish peroxidase compound II, J. Biol. Inorg. Chem. 1 (1996) 460–467, https://doi.org/10.1007/s007750050079.
[63] W. Sun, X. Ji, L.J. Kricka, H.B. Dunford, Rate constants for reactions of horseradish peroxidase compounds I and II with 4-substituted arylboronic acids, Can. J. Chem. 72 (1994) 2159–2162, https://doi.org/10.1139/v94-274.
[64] A. Henriksen, A.T. Smith, M. Gajhede, The structures of the horseradish peroxidase C-ferulic acid complex and the ternary complex with cyanide suggest how peroxidases oxidize small phenolic substrates, J. Biol. Chem. 274 (1999) 35005–35011, https://doi.org/10.1074/jbc.274.49.35005.